TPPB modulates PKC activity to attenuate neuroinflammation and ameliorate experimental multiple sclerosis

Shruthi Shanmukha[1], Wesley H. Godfrey[2], Payam Gharibani[2], Judy J. Lee[2], Yu Guo[3], Xiaojing Deng[2], Paul A. Wender[4], Michael D. Kornberg[2] and Paul M. Kim[1]*

[1]Department of Psychiatry and Behavioral Sciences, Johns Hopkins University School of Medicine, Baltimore, MD, United States, [2]Department of Neurology, Johns Hopkins University School of Medicine, Baltimore, MD, United States, [3]Department of Biomedical Engineering, Johns Hopkins University School of Medicine, Baltimore, MD, United States, [4]Departments of Chemistry and Chemical and Systems Biology, Stanford University, Stanford, CA, United States

Protein kinase C (PKC) plays a key role in modulating the activities of the innate immune cells of the central nervous system (CNS). A delicate balance between pro-inflammatory and regenerative activities by microglia and CNS-associated macrophages is necessary for the proper functioning of the CNS. Thus, a maladaptive activation of these CNS innate immune cells results in neurodegeneration and demyelination associated with various neurologic disorders, such as multiple sclerosis (MS) and Alzheimer's disease. Prior studies have demonstrated that modulation of PKC activity by bryostatin-1 (bryo-1) and its analogs (bryologs) attenuates the pro-inflammatory processes by microglia/CNS macrophages and alleviates the neurologic symptoms in experimental autoimmune encephalomyelitis (EAE), an MS animal model. Here, we demonstrate that (2S,5S)-(E,E)-8-(5-(4-(trifluoromethyl)phenyl)-2,4-pentadienoylamino)benzolactam (TPPB), a structurally distinct PKC modulator, has a similar effect to bryo-1 on CNS innate immune cells both *in vitro* and *in vivo*, attenuating neuroinflammation and resulting in CNS regeneration and repair. This study identifies a new structural class of PKC modulators, which can therapeutically target CNS innate immunity as a strategy to treat neuroinflammatory and neurodegenerative disorders.

KEYWORDS

multiple sclerosis, PKC modulator, remyelination, neuroinflammation, innate immunity, neurodegeneration

Introduction

Aberrant neuroinflammation by the innate immune cells of the central nervous system (CNS) contributes significantly to demyelination and neurodegeneration in multiple sclerosis (MS) and other neurologic disorders, e.g., Alzheimer's disease (AD), Parkinson's disease, and amyotrophic lateral sclerosis (Kutzelnigg and Lassmann, 2014; Hickman et al., 2018; Reich et al., 2018; Xie et al., 2022). In progressive MS, where the adaptive immune response plays a less prominent role, microglia and CNS-associated macrophages are activated in a pro-inflammatory phenotype that promotes demyelination and neurodegeneration (Mahad

et al., 2015; Voet et al., 2018; Faissner et al., 2019). Current Food and Drug Administration (FDA)-approved MS drugs primarily target peripheral lymphocytes and thus are effective in treating relapsing–remitting MS. However, these drugs inadequately address the disease progression and treatment of progressive MS by failing to modulate CNS innate immune cells. Therefore, compounds that therapeutically target CNS innate immunity to promote remyelination and CNS repair are greatly needed.

Protein kinase C (PKC) is a family of important signaling molecules that are involved in numerous cellular activities (Platten et al., 2003; Noh et al., 2012; Chen et al., 2014; Newton, 2018). Studies have demonstrated that the PKC isoforms in innate immune cells are important in key functions for stimulating CNS regeneration and repair, such as phagocytosis, secretion of neurotrophic factors, and providing supportive milieu (Zheleznyak and Brown, 1992; Hortelano et al., 1993; Smith et al., 1998; Fronhofer et al., 2006; Kooij et al., 2015; Lim et al., 2015). PKC is also a key signaling molecule in the triggering receptors expressed on myeloid cells 2 (TREM2) pathway, which is involved in critical microglia activities (Ulland and Colonna, 2018; Andreone et al., 2020; Kim and Kornberg, 2022; Wang et al., 2022). Thus, deletion or inhibition of this signaling pathway results in harmful outcomes. People with TREM2 missense mutation, Nasu-Hakola disease, experience an early onset of dementia and severe demyelination (Tanaka, 2000; Dardiotis et al., 2017).

We recently demonstrated that modulation of PKC activity hinders pro-inflammatory responses from microglia and macrophages, while activating anti-inflammatory and regenerative responses from these cells (Kornberg et al., 2018; Abramson et al., 2021; Gharibani et al., 2023). In experimental autoimmune encephalomyelitis (EAE), an MS animal model, modulation of PKC activity prevented the development of neurologic symptoms, and therapeutic treatment of EAE mice with a PKC modulator significantly improved the symptoms of EAE. Surprisingly, even in very late-stage EAE, when the peripheral inflammatory process has mostly subsided and only CNS inflammation persists, PKC modulation continued to ameliorate EAE symptoms. We also demonstrated using a lysolecithin (LPC)-induced demyelination model that modulation of PKC activity in microglia and CNS macrophages promoted remyelination by activating a regenerative phenotype in these cells, which provided a favorable anti-inflammatory environment, enhanced phagocytosis, and released beneficial factors to stimulate oligodendrocyte (OL) differentiation.

Our previous studies have focused primarily on modulating PKC activity with bryostatin-1 (bryo-1) and bryostatin analogs, termed bryologs (Abramson et al., 2021). Bryo-1, a natural compound that is CNS-penetrant and is a potent PKC modulator (Wender et al., 1988; Sun and Alkon, 2006; Hongpaisan et al., 2011), was originally tested as a cancer drug because it inhibited the tumorigenic properties of phorbol esters, which activate PKC (Clamp and Jayson, 2002), and since then, bryo-1 has also been tested for other indications, including AD, immunotherapy augmentation, and HIV eradication (Bullen et al., 2014; Laird et al., 2015; Gutiérrez et al., 2016; Farlow et al., 2019; Hardman et al., 2020; Sloane et al., 2020). We established that bryologs have similar biological effects as natural bryo-1 on innate immune cells. We also demonstrated that bryologs alleviated the symptoms of EAE and that the activity of bryo-1 and its analogs require PKC binding. Furthermore, our initial study showed that prostratin and prostratin analogs also had similar effects in cultured macrophages (Abramson et al., 2021),

indicating that other PKC modulators with chemical structures distinctly different from bryo-1 and bryologs may have therapeutic potential in treating neuroinflammatory and neurodegenerative disorders.

Here, we explored further the therapeutic potential of a structurally novel PKC modulator in stimulating an anti-inflammatory/regenerative phenotype in innate immune cells and in enhancing remyelination. We have identified (2S,5S)-(E,E)-8-(5-(4-(trifluoromethyl)phenyl)-2,4-pentadienoylamino)benzolactam (TPPB) (Kozikowski et al., 1997; Irie et al., 2005; Yi et al., 2012), a benzolactam that, while structurally different from bryo-1 and prostratin, binds to the C1 domain of PKC and has similar anti-inflammatory effects as bryo-1 and prostratin in cultured microglia and macrophages. We also demonstrate that TPPB, but not prostratin, improved EAE symptoms like bryo-1 and enhanced OL differentiation in a focal demyelination model. Our findings demonstrate that (1) TPPB has similar *in vitro* and *in vivo* effects to bryo-1 and (2) *in vitro* screening techniques allow for rapid screening of potential PKC modulators, but *in vivo* models, e.g., EAE and/or LPC-induced demyelination models, are required to establish the clinical potential of these compounds.

Materials and methods

Mice

Wild-type C57BL/6 J mice were purchased from the Jackson Laboratory (stock #000664). Animals were housed in a Johns Hopkins animal facility and acclimatized in the facility for at least 1 week. All animal experimental protocols were approved by the Johns Hopkins Institutional Animal Care and Use Committee.

Induction and scoring of EAE

EAE was induced in 8-12-week-old C57BL/6 J female mice by subcutaneous immunization of myelin oligodendrocyte glycoprotein 35–55 peptide (MOG_{35-55}). Briefly, 100 μg MOG_{35-55} was emulsified with 100 μl complete Freund's adjuvant, and 50 μl of the emulsion was subcutaneously injected into each of two sites on the lateral abdomen on day 0. Additionally, on day 0 and day 2, mice received 250 ng of pertussis toxin intraperitoneally (IP). Clinical signs of EAE were assessed daily beginning on day 7 post-immunization. Scoring was performed in a blinded manner according to the following scale: 0, no clinical deficit; 0.5, partial loss of tail tone; 1.0, complete tail paralysis or both partial loss of tail tone plus awkward gait; 1.5, complete tail paralysis and awkward gait; 2.0, tail paralysis with hind limb weakness evidenced by foot dropping between bars of cage lid while walking; 2.5, hind limb paralysis with little to no weight-bearing on hind limbs (dragging), but with some movement possible in legs; 3.0, complete hind limb paralysis with no movement in lower limbs; 3.5, hind limb paralysis with some weakness in forelimbs; 4.0, complete tetraplegia but with some movement of head; 4.5, moribund; and 5.0, dead.

Treatment of mice with TPPB and SUW014

TPPB (Tocris, 5343) and SUW014 (provided by P.A.W.) were dissolved in DMSO to 1 mM stock solutions, which were further

diluted to a desired concentration in sterile PBS for animal experiments. Mice were treated 3 days per week by IP injection of TPPB (50 nmol/kg), SUW014 (35 nmol/kg), or an equal volume of vehicle control. Mice were randomized and received their first treatment on the day they reached a clinical score of 1.0 or greater; thereafter, a three-days/week treatment schedule was followed.

Preparation of tissue for flow cytometry

Mice were euthanized with an overdose of isoflurane and then perfused with ice-cold PBS delivered via a cardiac puncture (Godfrey et al., 2023). Spinal cords were mechanically dissociated, then chemically dissociated with collagenase (200 U/ml) and DNase (100 U/ml) with constant shaking for 10 min, triturated with a pipette, and incubated for an additional 10 min. Cells were then passed through a 100-μm filter and washed with PBS. Myelin debris was removed by resuspending the cell pellet with a debris removal solution (Miltenyi Biotec), overlaying with PBS, and spinning at 3,000 g, and then removing the myelin debris layer. Cell pellets were resuspended in PBS, passed through a 100-μm filter, and stained with antibody as described below. Myeloid cell panels proceeded immediately to flow cytometry staining after cell isolation. For panels involving T cell cytokines, cells were first resuspended in a solution of complete RPMI with brefeldin/monensin and PMA/ionomycin for 4 h at 37°C.

Flow cytometry staining

All staining was performed in the dark at room temperature (RT). Cells were first stained with zombie NIR (1:1,500) for 10 min along with CD16/32 (1:100) dissolved in PBS. Cells were then washed and resuspended in a solution of PBS + 2% FBS + 1 mM EDTA and stained with the relevant antibodies. All surface antibodies were stained at a 1:300 dilution. Cells were then washed and incubated in FoxP3 fixation/permeabilization buffer following the manufacturer recommended protocol. Intracellular staining was performed with conjugated antibodies (1:200) against the specified proteins in permeabilization buffer for 1 h, washed twice, and then analyzed cells with a Cytek Aurora Flow cytometer. Data analysis was performed with FlowJo software.

Isolation and treatment of murine bone marrow-derived macrophages

Briefly, 8-10-week-old C57BL/6 J mice were euthanized, and bone marrow cells were isolated from their femurs in an aseptic environment by flushing with sterile PBS. The cell pellet was then collected by centrifugation (1,500 rpm for 8 min). The red blood cells (RBC) were lysed in RBC lysis buffer, followed by centrifugation (1,500 rpm for 8 min). The resulting cell pellet was resuspended in RPMI media supplemented with 10% FBS, 1% penicillin/streptomycin, 2 mM L-glutamine, 50 μM 2-mercaptoethanol, and 20 ng/ml recombinant mouse GM-CSF (Peprotech). The cells were incubated at 37°C for 7 days to induce macrophage differentiation. Subsequently, on day 8, bone marrow-derived macrophages (BMDM) were replated and treated as needed for the experiments. For treatment of cultured

cells, TPPB was dissolved in DMSO to a final concentration of 1 mM, which was subsequently dissolved in PBS or cell culture media for the required treatment. An equal volume of DMSO diluted in PBS or cell culture media was used as vehicle control.

Enzyme-linked immunosorbent assay

Bone marrow-derived macrophages were treated overnight with LPS (100 ng/ml) with or without TPPB (100 nM). Culture supernatants were collected, and cytokine production was assessed using enzyme-linked immunosorbent assay (ELISA) kits for IL-12 (88-7121-22), and IL-10 (88-7105-22) purchased from eBioscience and following the manufacturer's instructions. Plates were read at 450 nm on a plate reader.

Western blot

BMDM were treated overnight with LPS (100 ng/ml) ± TPPB (100 nM) or IL-4 (20 ng/ml) ± TPPB (100 nM). Cells were lysed in RIPA buffer supplemented with protease inhibitors, and protein concentration was determined by BCA assay. Protein samples were then prepared in SDS sample buffer and resolved by SDS/polyacrylamide gel electrophoresis. The bands were transferred to PVDF Immobilon-P membranes (Millipore) and blocked in TBS-T containing 5% BSA for 1 h at RT. The membranes were probed overnight at 4°C with rabbit monoclonal antibodies against inducible nitric oxide synthase (iNOS; Cell Signaling Technology, 2982) or arginase-1 (Arg-1; Cell Signaling Technology, 93668), followed by incubation with horseradish peroxidase (HRP) conjugated with anti-rabbit secondary antibodies (Cell Signaling Technology, 7074). Protein was detected with SuperSignal chemiluminescent substrate solution (Pierce), and Western blots were visualized using the LI-COR imaging system. The protein loading of each sample was verified by stripping the membrane with Restore Western blot stripping buffer, blocked again as described above, probed for 1 h at RT with HRP-conjugated anti-actin antibody (GeneScript, A00730), and visualized the protein expression as described earlier. The Western blot was quantified using ImageJ software.

In vitro phagocytosis assay with *Escherichia coli* bioparticles in BMDM

BMDM were treated overnight with LPS (100 ng/ml) with or without TPPB (100 nM). This was followed by aspirating the culture medium, and 100 μl of pHrodo Green *E. coli* BioParticles (ThermoFisher Scientific, P35366l) suspended in culture media were added to BMDM at a concentration of 50 bioparticles per cell. The cells were incubated for 3 h at 37°C in a humidified atmosphere of 5% CO_2, washed twice with sterile PBS, and then incubated with 100 μl of diluted trypan blue with PBS (1:2 dilution) to quench the extracellular fluorescence. The cells were washed twice with PBS fixed with 100 μl of 4% paraformaldehyde (PFA), incubated for 15 min at RT, and washed with PBS (100 μl per well for each wash). Following the wash step, 50 μl of PBS was added to each well, and fluorescence intensity was measured on a SpectraMax fluorescent plate reader. The

phagocytosis was calculated as a percentage relative fluorescence intensity normalized to cell number.

Myelin isolation and in-cell Western blot (ICW) for myelin phagocytosis in BMDM

Myelin isolation

Myelin isolation and labeling with carboxyfluorescein succinimidyl ester (CFSE) were performed as previously described (Rolfe et al., 2017), and 8-10-week-old C57BL/6 J mice were used to isolate myelin. Briefly, the whole brains were dissected from euthanized animals and homogenized using a sterile hand-held rotary homogenizer in ice-cold 0.32 M sucrose solution. The homogenate was carefully overlaid onto ice-cold 0.83 M sucrose solution in a 50-ml polypropylene centrifuge tube, forming a sucrose density gradient, and centrifuged at 100,000 g at 4°C for 45 min in a pre-cooled ultracentrifuge rotor. The resulting white crude myelin interface was collected from the interface between two sucrose densities and further homogenized in a sterile hand-held rotary homogenizer for 30–60 s before subjecting to centrifugation at 100,000 g at 4°C for 45 min in a pre-cooled ultracentrifuge rotor. The solid white myelin pellet was resuspended in Tris-Cl solution and centrifuged at 100,000 g at 4°C for 45 min. Subsequently, the pellet was resuspended in sterile PBS and centrifuged at 22,000 g for 10 min at 4°C. The final isolated myelin pellet was resuspended in sterile PBS to a final concentration of 100 mg/ml.

Myelin labeling

For CFSE labeling, 10 mg of myelin was resuspended in 200 μl of 50 μM CFSE and incubated at RT for 30 min in the dark, followed by centrifugation at 14,800 g for 10 min at 4°C. The pellet containing labeled myelin was washed in 100 mM glycine in PBS for three times and resuspended in sterile PBS.

ICW for myelin phagocytosis in BMDM

BMDM were cultured on a clear bottom 96-well cell culture plate at a density of 2.5×10^4 cells per well. The cells were treated with either vehicle or TPPB (100 nM) for 3 h, followed by incubation with 1 mg/mL of CFSE-labeled myelin for overnight at 37°C. BMDM were washed several times with sterile PBS to remove non-engulfed myelin debris. The cells were fixed with 4% PFA for 15 min and incubated with 0.1% Triton X-100 in PBS for 10 min. The fixed cells were incubated for 2 h at RT with β-actin antibody (Cell Signaling Technology, 4967) at 1:1,000 dilution and then incubated with VRDye 549 Goat anti-Rabbit IgG Secondary Antibody (LI-COR biosciences, 926-54020) for 30 min. The plates were scanned on the LI-COR Odyssey imaging system according to the manufacturer's protocol. Myelin phagocytosis by BMDM is represented as the total fluorescence intensity of CFSE-myelin and normalized to the fluorescence intensity measured for β-actin for each well on ImageJ.

Focal spinal cord demyelination

LPC-induced demyelination

Focal demyelination was induced in 8–12-week-old C57BL/6 J mice by injecting 1% LPC (Sigma) in PBS into the ventral funiculus as described previously (Gharibani et al., 2023). Briefly, mice were anesthetized with ketamine (100 mg/kg) and xylazine (10 mg/kg) injected IP. Mice were placed on a stereotaxic frame, and a small midline incision was made below the ears on the back of the animal in the caudal direction. The prominent T2 was used as a landmark to expose the spinal cord and identify T3-4 intervertebral space. The dura was removed with a 32G needle without damaging the tissues. LPC (0.5 μl) was microinjected stereotaxically, at a rate of 0.25 μl/min using a microinjection syringe pump (UMP3; World Precision Instrument), into the right ventral funiculus (depth of 1.3 mm) via a 34G needle (Hamilton Co.) connected to a 10 μl Hamilton syringe. To avoid LPC efflux, there was a 2-min pause after LPC injection before retracting the needle. A single absorbable suture (Vicryl 5-0) was used to close the muscle and adipose tissues, following which the skin incision was closed with rodent wound clips. Saline (1 ml) and buprenorphine SR (1 mg/kg; ZooPharm, LLC) were administered subcutaneously after the surgery to prevent dehydration and pain, respectively. Gentamycin (2 mg/kg; Henry Schein Animal Health) was given subcutaneously every 12 h for 3 days. Treatment with TPPB (50 nmol/kg, three times a week) or vehicle started 48 h after the surgery by IP injection.

Spinal cord harvest

The animals were anesthetized and transcardially perfused with PBS briefly, followed by ice-cold 4% PFA (Sigma). Spinal cord tissues were then harvested and made into a 3-mm piece of lesion site with the epicenter (site of injection) in the middle. The tissues were kept in 4% PFA at 4°C overnight for post-fixation, followed by cryoprotection in gradient sucrose (10% then 30% sucrose in PBS at 4°C overnight). The tissues were then embedded in O.C.T. and were coronally sectioned into 12-μm thickness sections at 0.8 mm from the epicenter at both sides (rostrally and caudally) using a cryostat (Thermo Shandon). The sections were collected on Superfrost Plus slides (VWR International) and stored at −80°C until staining.

Immunofluorescence staining

The spinal cord sections were retrieved by Universal Antigen Retrieval Kit (R&D Systems) in a steamer for 15 min at 100°C, permeabilized with 1% Triton X-100 in TBS for 5 min, and incubated in blocking solution (10% donkey serum, 0.25% Triton X-100 in TBS) for 1 h at RT. Primary antibodies were diluted in blocking solution and incubated for two overnights at 4°C. In order to study OL differentiation, double staining was performed with rabbit anti-Olig2 (1:100; Millipore) and mouse anti-APC (CC1; 1:100; Sigma). This was followed by incubating with appropriate fluorochrome-conjugated secondary antibodies (1:500; Thermo Fisher Scientific) for 2 h at RT, counterstaining with DAPI (3 μM in PBS; Sigma), and covering with antifade mounting media before placing coverslips. Minimum of six sections (3 rostral and 3 caudal) were counted manually by investigators who were blinded to the study groups. The total numbers of positive cells were normalized to the area of the injury using ImageJ.

Results

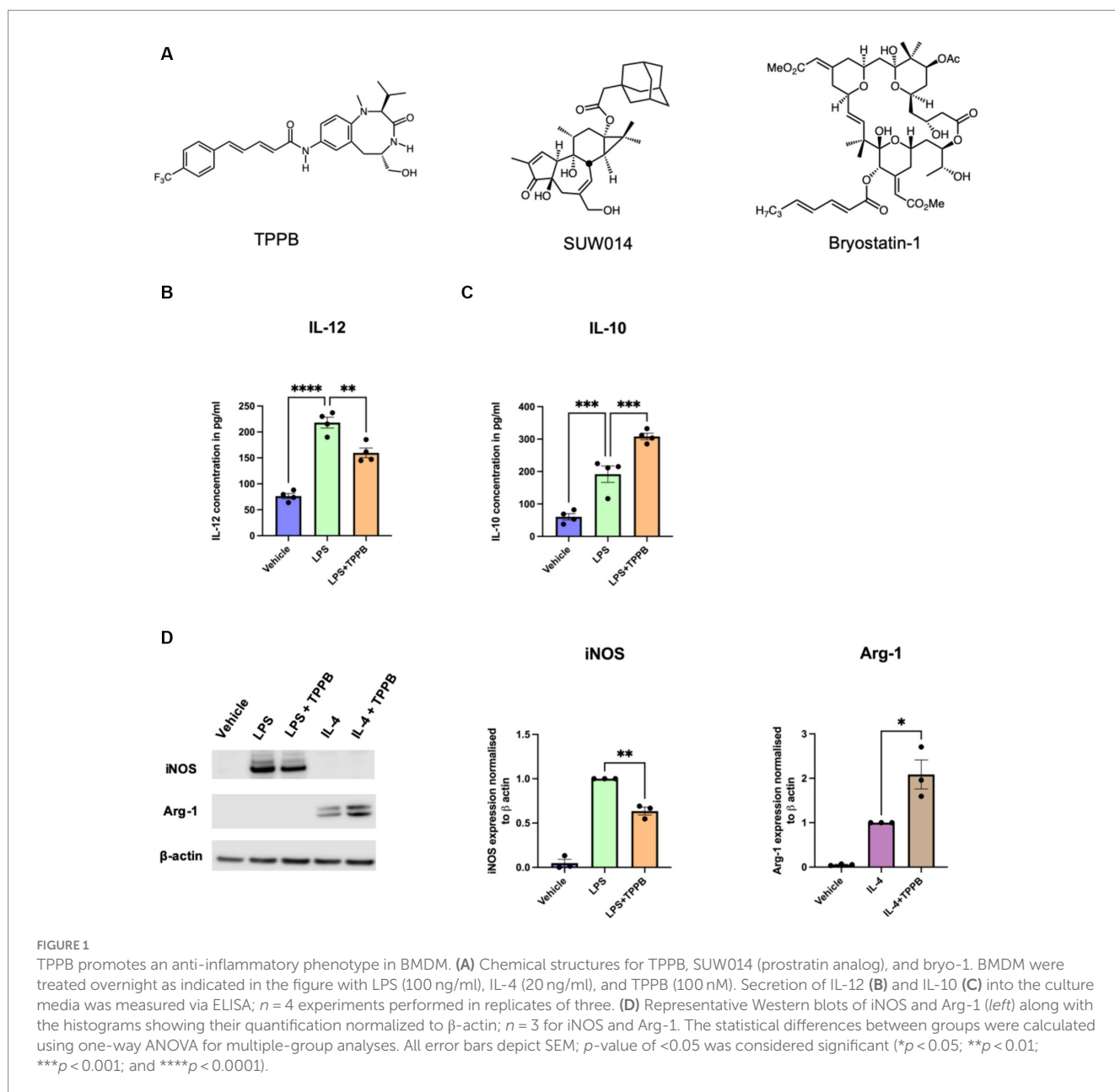### TPPB induces an anti-inflammatory phenotype in BMDM

We have previously demonstrated that the PKC modulator bryo-1 promotes anti-inflammatory/regenerative activation of macrophages

while concurrently suppressing pro-inflammatory markers in myeloid cells (Kornberg et al., 2018; Abramson et al., 2021). We also showed that the structurally unrelated PKC modulator SUW014, an analog of prostratin, exhibits bryo-1-like effects on myeloid cells, suggesting that these and related PKC modulators may serve as candidate drugs for targeting the innate immune cells in CNS. Here, we aimed to determine the anti-inflammatory potential of TPPB (Figure 1A), a cell-permeable high-affinity PKC modulator, on peripheral BMDM. BMDM were stimulated with LPS (100 ng/ml) for 24 h with or without treatment with TPPB (100 nM), and cytokine secretion in the cell culture supernatant was examined by ELISA. Treatment with TPPB significantly inhibited the production of the pro-inflammatory cytokine IL-12 induced by LPS (Figure 1B) and increased the secretion of the anti-inflammatory cytokine IL-10 (Figure 1C). Furthermore, TPPB inhibited the expression of iNOS, a key marker of pro-inflammatory phenotype, induced by LPS and augmented the

expression of Arg-1, a marker of anti-inflammatory/regenerative phenotype, after IL-4 stimulation (Figure 1D). The purity and specific expression of iNOS and Arg-1 in BMDM are demonstrated in Supplementary Figures S1, S2. Overall, these data suggest that TPPB promotes the activation of macrophages that are involved in the regulation of the immune responses to limit inflammation and promote tissue repair mechanisms.

TPPB attenuates neurologic deficits in EAE

Our previous study demonstrated that bryo-1 attenuated the development and progression of EAE, and thus, bryo-1 represented a potential therapeutic agent for MS (Kornberg et al., 2018; Abramson et al., 2021). Similarly, having evaluated the anti-inflammatory effect of TPPB *in vitro*, we used the EAE model to carry out *in vivo*

FIGURE 1
TPPB promotes an anti-inflammatory phenotype in BMDM. **(A)** Chemical structures for TPPB, SUW014 (prostratin analog), and bryo-1. BMDM were treated overnight as indicated in the figure with LPS (100 ng/ml), IL-4 (20 ng/ml), and TPPB (100 nM). Secretion of IL-12 **(B)** and IL-10 **(C)** into the culture media was measured via ELISA; $n = 4$ experiments performed in replicates of three. **(D)** Representative Western blots of iNOS and Arg-1 (*left*) along with the histograms showing their quantification normalized to β-actin; $n = 3$ for iNOS and Arg-1. The statistical differences between groups were calculated using one-way ANOVA for multiple-group analyses. All error bars depict SEM; p-value of <0.05 was considered significant (*$p < 0.05$; **$p < 0.01$; ***$p < 0.001$; and ****$p < 0.0001$).

investigations of TBBP to better understand its clinical potential. MOG_{35-55}-induced EAE model was used, and drug treatment began when the animals demonstrated EAE symptoms (clinical score of at least 1). In this experiment, we also tested prostratin analog SUW014, which was not done in the previous study (Abramson et al., 2021). We discovered that SUW014 (35 nmol/kg) had no effect on attenuating EAE symptoms when administered IP 3 days a week, and both vehicle- and SUW014-treated mice progressively developed neurologic symptoms (Figure 2A). On the other hand, TPPB (50 nmol/kg) attenuated the clinical symptoms of EAE and showed lower peak clinical score when administered IP 3 days per week at the onset of symptoms (Figure 2B). These results suggest that TPPB, like bryo-1, provides a beneficial effect on EAE mice and serves as a promising candidate for MS treatment.

TPPB suppresses CNS inflammation in EAE

To better understand the beneficial effect of TPPB on EAE, we examined the impact of TPPB on myeloid and lymphoid cell phenotypes in the CNS at peak EAE using flow cytometry. MOG_{35-55}-induced EAE mice were treated with vehicle or TPPB (50 nmol/kg, 3 days per week) at the onset of clinical symptoms, and analyses were performed at peak disease on post-immunization day (PID) 19. Flow cytometry analyses revealed that treatment with TPPB suppressed CNS inflammation as demonstrated by a reduction in the population of $CD11b^+CD45^+$ cells expressing MHC class II in the spinal cord of EAE mice compared to the vehicle-treated group (Figure 3A). Furthermore, TPPB increased the population of $CD11b^+CD45^+CD206^+$ cells in the spinal cord, suggesting that TPPB favors the activation of an anti-inflammatory phenotype (Figure 3B). In addition, there was a significant downregulation in the proportion of CD4 lymphocytes displaying IL-17 ($CD4^+IL-17^+$) in the TPPB-treated group compared to the vehicle group, which indicates an efficient alleviation of inflammation by TPPB (Figure 3C). The gating strategy and representative negative control for flow cytometry for this experiment are shown in Supplementary Figure S3. Overall, these results demonstrate that TPPB has a profound protective effect on the immune response in the MOG_{35-55}-induced EAE model of MS.

TPPB potentiates the repair mechanism by enhancing phagocytosis

Having evaluated the potential of TPPB in the resolution of inflammation both in cultured BMDM and EAE animal model, we next sought to better understand the impact of TPPB on repair mechanisms by investigating its effect on phagocytosis. Phagocytosis is a key function of innate immune cells during remyelination by removing the deleterious and inhibitory myelin debris for an effective OL differentiation to occur. For the phagocytosis assay, BMDM were treated with either vehicle or TPPB (100 nM) for 24 h, and then were incubated with pHrodo *E. coli* BioParticles for 3 h followed by the measurement of relative fluorescence intensity on a plate reader. Compared to the vehicle condition, TPPB-treated group showed a significantly higher percentage of relative fluorescence intensity, suggesting increased phagocytosis when BMDM were treated with TPPB (Figure 4A). In addition, we performed a phagocytosis assay with CFSE-tagged myelin, where the BMDM were cultured on clear bottom 96-well plates and treated with either vehicle or TPPB (100 nM), followed by overnight incubation with CFSE-tagged myelin. ICW was performed to visualize the phagocytosed myelin, and β-actin staining was used to normalize the data (Figure 4B). Treatment of BMDM with TPPB significantly increased the phagocytosis of myelin (Figure 4C). The results from this experiment confirm that, in addition to the significant anti-inflammatory effect, TPPB also potentiates repair functions by promoting phagocytosis in innate immune cells.

TPPB increases OL differentiation following focal demyelination

To evaluate the remyelination potential of TPPB in MS, we used the LPC-induced focal demyelination model. Focal demyelination was induced in the ventral spinal cord of the mice by stereotaxic injection of LPC. Treatment with TPPB (50 nmol/kg, 3 days/week) or vehicle was initiated 48 h post-LPC injection for 2 weeks. Representative images of lesions from 15 days post-lesion (dpl) in the TPPB- and vehicle-treated mice stained for $Olig2^+$, $CC1^+$, and DAPI are shown in Figure 5A. The number of total OL-lineage cells ($Olig2^+$) did not change with TPPB treatment (Figure 5B). However, the number of the
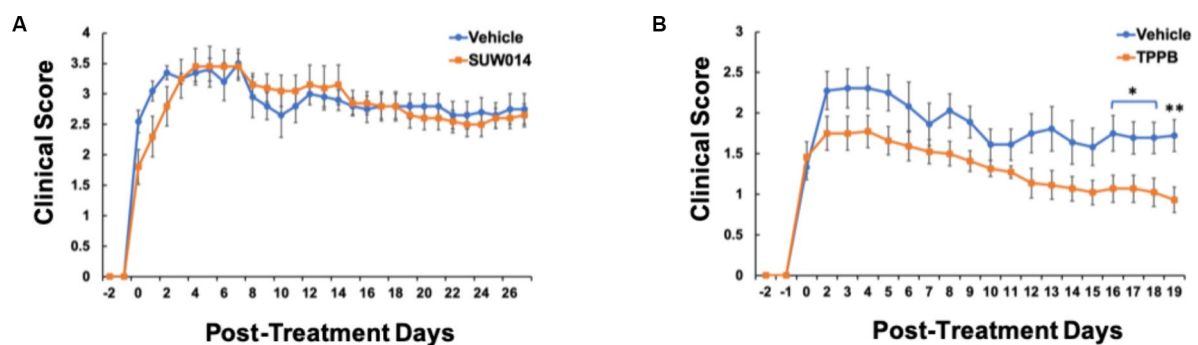

FIGURE 2
TPPB attenuates neurologic deficits in MOG_{35-55}-induced EAE mice. Mice were treated with SUW014 (A) and TPPB (B) by IP injection three times a week at the onset of EAE symptoms. TBBP significantly ameliorated the neurologic symptoms of EAE, but SUW014 did not improve the symptoms. Data represent mean ± SEM; $n = 5$ for vehicle and SUW014 (A) and $n = 9$ and 11 for vehicle and TPPB (B), respectively. Statistical significance was determined by a two-tailed Student's *t*-test for EAE clinical score; *p*-value of <0.05 was considered significant (*$p < 0.05$ and **$p < 0.01$).
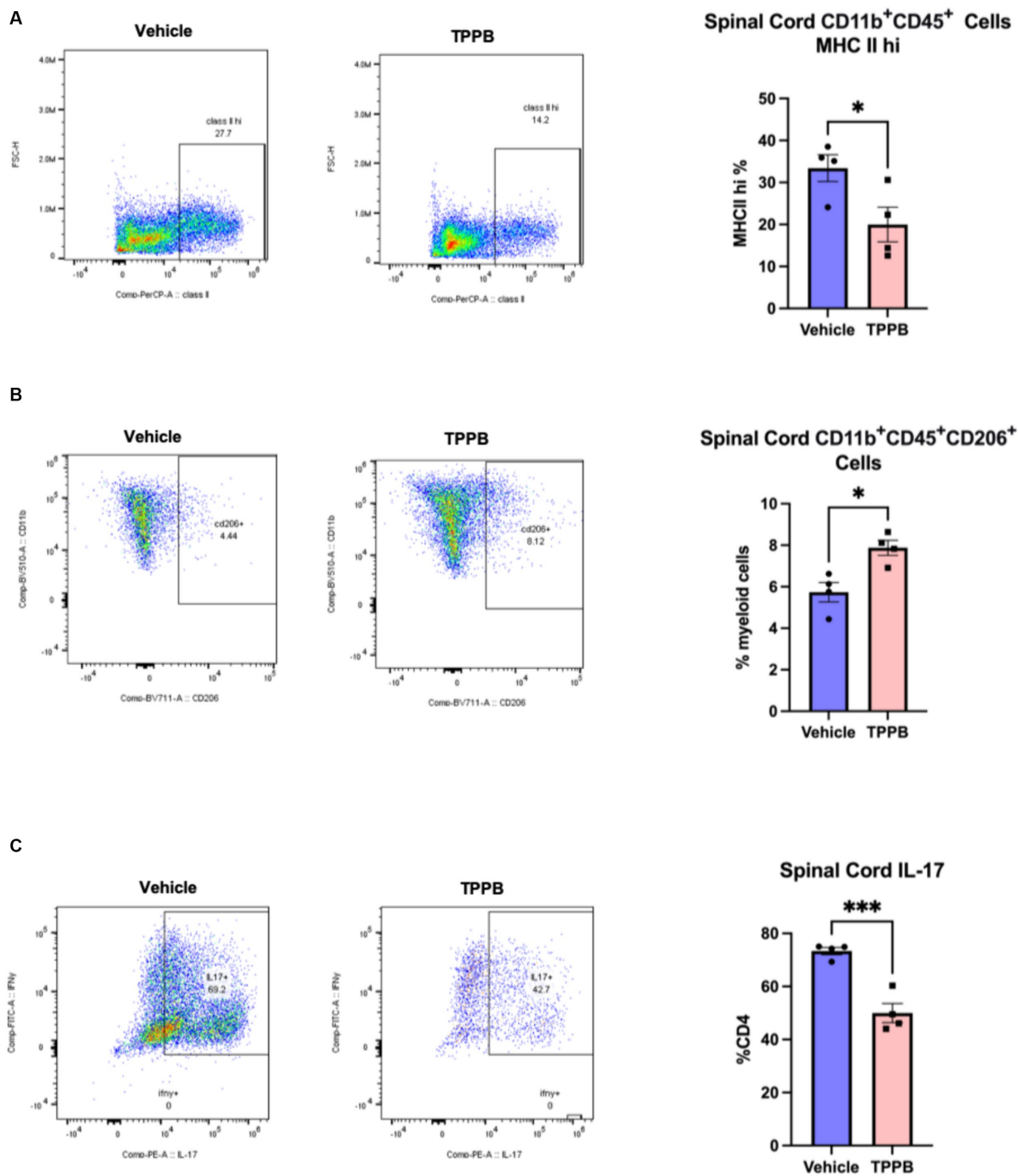
FIGURE 3

TPPB suppresses CNS inflammation in EAE mice. MOG_{35-55}–induced EAE mice were treated with TBBP (50 nmol/kg, 3 days/week) or vehicle when neurologic symptoms first appeared, and they were sacrificed on PID 19. **(A)** Flow cytometry dot plots indicate the infiltrating $CD11b^+CD45^+$ cells examined for expression of MHC II and gated for MHC II^{hi} cells in the spinal cords of the EAE mice (*left*). The bar graph (*right*) shows the decreased percentage of these cells in the TPPB-treated group as compared to the vehicle control group. **(B)** Flow cytometry dot plots show $CD11b^+CD45^+CD206^+$ cells as percentage of $CD11b^+CD45^+$ cells in the spinal cord (*left*), and the bar graph (*right*) demonstrates the increase in the percentage of these cells in EAE mice treated with TPPB. **(C)** Flow cytometry dot plots show the expression of IL-17$^+$ cells as percentage of total $CD4^+$ T cells in the spinal cord of EAE animals (*left*), with the bar graph (*right*) indicating significant reduction in IL-17$^+$ cells as a percentage of $CD4^+$ T cells in the TPPB-treated group. $n = 4$ for flow cytometry. All error bars represent SEM. Statistical significance was determined by a two-tailed Student's t-test for flow cytometry data; p-value of <0.05 was considered significant (*$p < 0.05$ and ***$p < 0.001$).

differentiating OL (Olig2$^+$CC1$^+$) within the lesions showed a trend towards increased differentiation in the TPPB-treated group when compared to the control group at 15 dpl (Figure 5C). The number of

differentiating OL (Olig2$^+$CC1$^+$) represented as a percentage of total Olig2$^+$ also showed a similar trend of increased OL differentiation in the TPPB-treated group (Figure 5D). Similar to bryo-1, this result
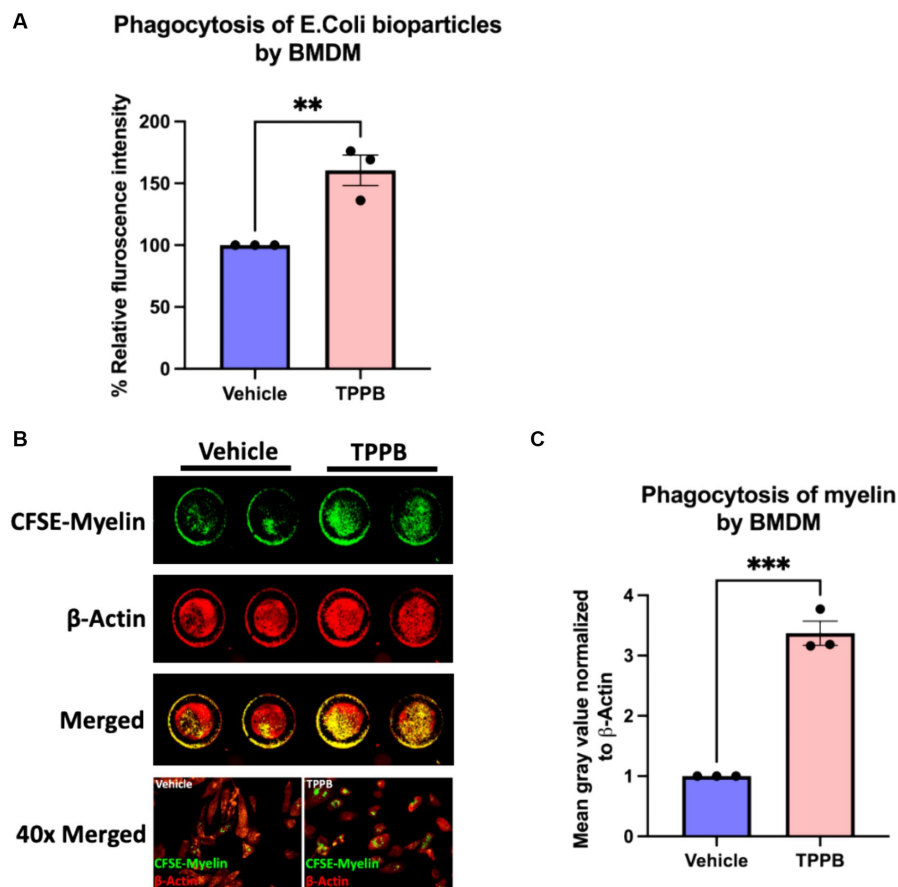
FIGURE 4
TPPB promotes phagocytosis in BMDM *in vitro*. **(A)** BMDM cells were cultured in a 96-well plate and treated with either vehicle or TPPB (100 nM) and then incubated with *E. coli* bioparticles for 3 h. Following this, the fluorescence intensity of phagocytosed *E. coli* particles was measured. The bar graph representing the percentage relative fluorescence intensity shows significantly increased phagocytic activity of BMDM against *E. coli* particles when treated with TPPB (100 nM) measured on a plate reader. All error bars depict SEM ($n = 3$). **(B)** Representative image of an ICW with representative 40x magnified images of BMDM phagocytosing myelin. BMDM cells were cultured in a 96-well plate and treated with either vehicle or TPPB (100 nM) followed by overnight incubation with CFSE-tagged myelin. β-actin expression was used as the control. **(C)** Calculated total fluorescence of ICW data quantified on ImageJ shows a significant increase in phagocytosis of CFSE-tagged myelin in the TPPB-treated group compared to the vehicle group. Quantification (mean $\pm$ SEM) from $n = 3$ and statistical significance were determined by a two-tailed Student's *t*-test; *p*-value of <0.05 was considered significant (**$p < 0.01$ and ***$p < 0.001$).

suggests TPPB's potential enhancement of OL differentiation, which is critical during remyelination (Gharibani et al., 2023).

Discussion

In our previous study, we demonstrated that our screening platform provided a rapid method for identifying PKC modulators for treating neuroinflammatory and neurodegenerative disorders (Abramson et al., 2021). That study showed that the prostratin analog SUW014 has a similar anti-inflammatory effect on cultured macrophages as bryo-1, and in this study, we have also identified TPPB as another potential PKC modulating compound with bryo-1-like properties. Our initial study primarily focused on bryo-1 and its analogs, but it did not further examine the *in vivo* effects of SUW014. Thus, to advance TPPB and/or SUW014 forward in our drug assay progression, we investigated the *in vivo* activity of these agents. We found that SUW014 interestingly did not ameliorate the neurologic symptoms of EAE, while TPPB was able to improve EAE phenotype

like bryo-1 and bryologs. We recently established that bryo-1 is able to activate phagocytosis in macrophages and microglia (which is critical during remyelination as myelin debris inhibits myelin formation) and enhance remyelination in LPC-induced demyelination model (Gharibani et al., 2023). Here, we also demonstrated that TPPB stimulates phagocytosis by macrophages and increases OL differentiation in focal LPC-induced demyelination animal model.

The results from this current study indicate that while the *in vitro* immunologic assays are a useful initial screening method to identify candidate compounds, *in vitro* assays are not sufficient. As is found in many preclinical studies, *in vitro* activities do not always correlate with *in vivo* effects – in this case, a compound's ability to mitigate neuroinflammation and promote remyelination. SUW014 demonstrates a greater potency than bryo-1 in triggering an anti-inflammatory response from *in vitro* macrophages, but it failed to alleviate EAE *in vivo*. While beyond the scope of this study but prompted by its findings, it would be important to determine why SUW014 was not able to treat the neurologic symptoms of EAE given that it had such promising *in vitro* activity. It is possible that SUW014 has poor bioavailability or was
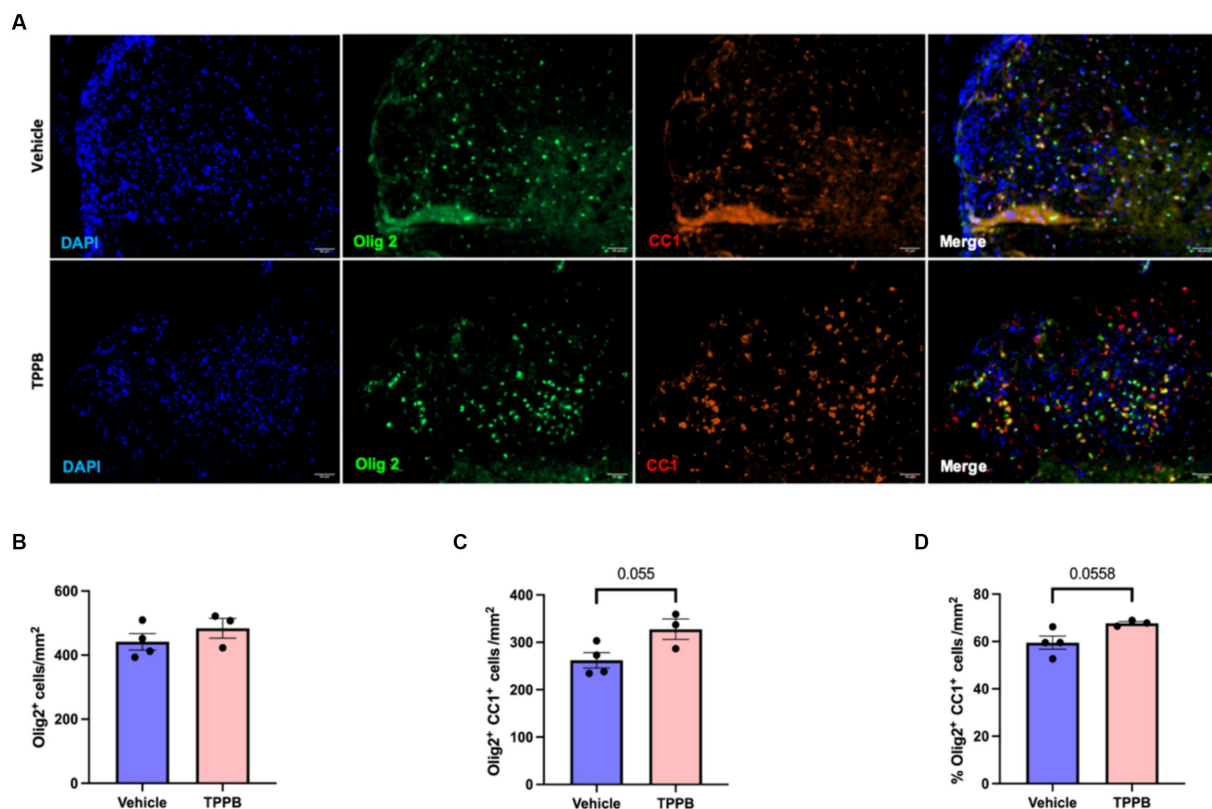
FIGURE 5
TPPB shows a trend towards enhancing OL differentiation following focal demyelination. **(A)** Representative images of LPC-induced demyelination lesions from 15 dpl in vehicle- and TPPB-treated mice stained for the shown markers. **(B)** Quantification of total OL-lineage cells (Olig2$^+$) shows no significant difference in the total number of Olig2$^+$ cells when treated with TPPB. **(C)** There is a trend towards increased differentiating OL (Olig2$^+$CC1$^+$) within the lesions at 15 dpl in TPPB-treated mice. **(D)** The bar graph shows the number of differentiating OL (Olig2$^+$CC1$^+$) represented as a percentage of Olig2$^+$ cells, which also demonstrates similar trend as the total number of differentiating OL **(B)**. Quantification (mean $\pm$ SEM) from $n = 4$ mice for vehicle and $n = 3$ mice for the TPPB group and statistical significance were determined by a two-tailed Student's t-test; p-value of <0.05 was considered significant.

not absorbed adequately when administered IP. It is also feasible that SUW014 did not reach a therapeutic concentration in the CNS or that the dosing regimen of three times a week is insufficient. Loss through metabolism is another potential contributing factor as SUW014 has an esterase-labile ester functionality while TPPB has more stable amide bonds. Therefore, *in vivo* ester loss would eliminate PKC binding. It is also possible that off-target associations by SUW014 might contribute to the observed *in vitro* versus *in vivo* differences.

The discovery that TPPB and bryo-1 have similar *in vitro* and *in vivo* activities has several important implications. Our results demonstrate that TPPB, which is a specific and potent PKC modulator like bryo-1, has immunomodulatory effects in an EAE model, enhances phagocytosis, and increases OL differentiation. Identification of TBBP also indicates that the anti-inflammatory and regenerative properties of innate immune cells depend on PKC activity and not off-target effects of bryo-1, as it is unlikely that both bryo-1 and TPPB have the same off-target activities to provide these beneficial effects on innate immune cells. Additionally, our previous study established that modification of bryo-1 so that it can no longer bind to PKC (SUW275) prevents anti-inflammatory effects in myeloid cells and does not ameliorate EAE symptoms (Abramson et al., 2021). Finally, having structurally different chemicals with similar functional effects on PKC and in animal models of MS allows for diversification of candidates, which increases the

probability of identifying the best candidate to advance forward in drug development for neuroinflammatory and neurodegenerative disorders.

PKC isoforms belongs to one of three classes, which are conventional (α, β, and γ), novel (δ, ε, η, and θ), and atypical (ζ and ι/λ). Conventional and novel PKCs have a C1 domain that binds to bryo-1, TPPB, and endogenous diacylglycerol (DAG), but atypical PKCs do not (Das and Rahman, 2014; Katti et al., 2022). Currently, it is unknown which isoform(s) is involved in anti-inflammatory and regenerative effects in microglia and CNS-associated macrophages. It is possible that TPPB intracellularly could activate more specifically the isoform(s) critical for immunomodulation of CNS innate immune cells, which would decrease the side effects that are typically observed with bryo-1, such as myalgia. The identification of PKC isoform(s) involved in this process and the specificity of TPPB and bryo-1 are under ongoing investigation.

Overall, we have discovered that TPPB, while significantly different in structure from bryo-1, has similar beneficial activities to bryo-1. This finding is consistent with their sharing common chemical properties that allow binding to PKC (Wender et al., 1986; Loy et al., 2015). TPPB serves as a new structural lead in an armamentarium of PKC-modulating drugs that could prove effective in the treatment of neuroinflammatory and neurodegenerative disorders for which there is a lack of therapeutic options. This study shows for the first time that the EAE activities of bryo-1 and its analogs are also exhibited *in vivo*

by a structurally distinct molecular class, thus creating another therapeutic options for targeting CNS innate immune cells to modulate neuroinflammation and to promote CNS regeneration and repair.

Data availability statement

The original contributions presented in the study are included in the article/Supplementary material, further inquiries can be directed to the corresponding author.

Ethics statement

The animal study was approved by The Johns Hopkins University School of Medicine. The study was conducted in accordance with the local legislation and institutional requirements.

Author contributions

Funding

Acknowledgments

Conflict of interest

The Johns Hopkins University has filed a patent for the application of PKC modulator bryo-1 and related technology, and PK and MK are co-inventors on the patent. MK has received consulting fees from Biogen, Genentech, Novartis, TG Therapeutics, and OptumRx. Stanford University has filed patents on bryostatin and other PKC modulators which have been licensed by Neurotrope BioScience for the treatment of neurological disorders and by Bryologyx Inc. for use in HIV/AIDS eradication and cancer immunotherapy. PW is an advisor to both companies and a cofounder of the latter.

The remaining authors declare that the research was conducted in the absence of any commercial or financial relationships that could be construed as a potential conflict of interest.

Publisher's note

All claims expressed in this article are solely those of the authors and do not necessarily represent those of their affiliated organizations, or those of the publisher, the editors and the reviewers. Any product that may be evaluated in this article, or claim that may be made by its manufacturer, is not guaranteed or endorsed by the publisher.

Supplementary material

The Supplementary material for this article can be found online at: https://www.frontiersin.org/articles/10.3389/fncel.2024.1373557/full#supplementary-material

References

Abramson, E., Hardman, C., Shimizu, A. J., Hwang, S., Hester, L. D., Snyder, S. H., et al. (2021). Designed PKC-targeting bryostatin analogs modulate innate immunity and neuroinflammation. *Cell Chem. Biol.* 28, 537–545.e4. doi: 10.1016/j.chembiol.2020.12.015

Andreone, B. J., Przybyla, L., Llapashtica, C., Rana, A., Davis, S. S., van Lengerich, B., et al. (2020). Alzheimer's-associated PLCγ2 is a signaling node required for both TREM2 function and the inflammatory response in human microglia. *Nat. Neurosci.* 23, 927–938. doi: 10.1038/s41593-020-0650-6

Bullen, C. K., Laird, G. M., Durand, C. M., Siliciano, J. D., and Siliciano, R. F. (2014). New ex vivo approaches distinguish effective and ineffective single agents for reversing HIV-1 latency in vivo. *Nat. Med.* 20, 425–429. doi: 10.1038/nm.3489

Chen, Z., Forman, L. W., Williams, R. M., and Faller, D. V. (2014). Protein kinase C-delta inactivation inhibits the proliferation and survival of cancer stem cells in culture and in vivo. *BMC Cancer* 14:90. doi: 10.1186/1471-2407-14-90

Clamp, A., and Jayson, G. C. (2002). The clinical development of the bryostatins. *Anti Cancer Drugs* 13, 673–683. doi: 10.1097/00001813-200208000-00001

Dardiotis, E., Siokas, V., Pantazi, E., Dardioti, M., Rikos, D., Xiromerisiou, G., et al. (2017). A novel mutation in TREM2 gene causing Nasu-Hakola disease and review of the literature. *Neurobiol. Aging* 53, 194.e13–194.e22. doi: 10.1016/j.neurobiolaging.2017.01.015

Das, J., and Rahman, G. M. (2014). C1 domains: structure and ligand-binding properties. *Chem. Rev.* 114, 12108–12131. doi: 10.1021/cr300481j

Faissner, S., Plemel, J. R., Gold, R., and Yong, V. W. (2019). Progressive multiple sclerosis: from pathophysiology to therapeutic strategies. *Nat. Rev. Drug Discov.* 18, 905–922. doi: 10.1038/s41573-019-0035-2

Farlow, M. R., Thompson, R. E., Wei, L. J., Tuchman, A. J., Grenier, E., Crockford, D., et al. (2019). A randomized, double-blind, placebo-controlled, phase II study assessing safety, tolerability, and efficacy of bryostatin in the treatment of moderately severe to severe Alzheimer's disease. *J. Alzheimers Disease* 67, 555–570. doi: 10.3233/JAD-180759

Fronhofer, V., Lennartz, M. R., and Loegering, D. J. (2006). Role of PKC isoforms in the FcγR-mediated inhibition of LPS-stimulated IL-12 secretion by macrophages. *J. Leukoc. Biol.* 79, 408–415. doi: 10.1189/jlb.0805438

Gharibani, A. P., Abramson, E., Shanukah, S., Smith, M. D., Godfrey, W. H., Lee, J. J., et al. (2023). PKC modulator bryostatin-1 therapeutically targets CNS innate immunity to attenuate neuroinflammation and promote remyelination. *bioRxiv*, 1–35. doi: 10.1101/2023.08.28.555084

Godfrey, W. H., Hwang, S., Cho, K., Shanmukha, S., Gharibani, P., Abramson, E., et al. (2023). Therapeutic potential of blocking GAPDH Nitrosylation with CGP3466b in experimental autoimmune encephalomyelitis. *Front. Neuro* 13:979659. doi: 10.3389/fneur.2022.979659

Gutiérrez, C., Serrano-Villar, S., Madrid-Elena, N., Pérez-Elías, M. J., Martín, M. E., Barbas, C., et al. (2016). Bryostatin-1 for latent virus reactivation in HIV-infected patients on antiretroviral therapy. *AIDS* 30, 1385–1392. doi: 10.1097/QAD.0000000000001064

Hardman, C., Ho, S., Shimizu, A., Luu-Nguyen, Q., Sloane, J. L., Soliman, M. S. A., et al. (2020). Synthesis and evaluation of designed PKC modulators for enhanced cancer immunotherapy. *Nat. Commun.* 11:1879. doi: 10.1038/s41467-020-15742-7

Hickman, S., Izzy, S., Sen, P., Morsett, L., and el Khoury, J. (2018). Microglia in neurodegeneration. *Nat. Neurosci.* 21, 1359–1369. doi: 10.1038/s41593-018-0242-x

Hongpaisan, J., Sun, M. K., and Alkon, D. L. (2011). PKC ε activation prevents synaptic loss, Aβ elevation, and cognitive deficits in Alzheimer's disease transgenic mice. *J. Neurosci.* 31, 630–643. doi: 10.1523/JNEUROSCI.5209-10.2011

Hortelano, S., Genaro, A. M., and Boscá, L. (1993). Phorbol esters induce nitric oxide synthase and increase arginine influx in cultured peritoneal macrophages. *FEBS Lett.* 320, 135–139. doi: 10.1016/0014-5793(93)80078-9

Irie, K., Nakagawa, Y., and Ohigashi, H. (2005). Indolactam and Benzolactam compounds as new medicinal leads with binding selectivity for C1 domains of protein kinase C isozymes. *Curr. Pharm. Des.* 10, 1371–1385. doi: 10.2174/1381612043384907

Katti, S. S., Krieger, I. V., Ann, J., Lee, J., Sacchettini, J. C., and Igumenova, T. I. (2022). Structural anatomy of protein kinase C C1 domain interactions with diacylglycerol and other agonists. *Nat. Commun.* 13:2695. doi: 10.1038/S41467-022-30389-2

Kim, P. M., and Kornberg, M. D. (2022). Targeting PKC in microglia to promote remyelination and repair in the CNS. *Curr. Opin. Pharmacol.* 62, 103–108. doi: 10.1016/J.COPH.2021.11.008

Kooij, G., Braster, R., Koning, J. J., Laan, L. C., van Vliet, S. J., Los, T., et al. (2015). *Trichuris suis* induces human non-classical patrolling monocytes via the mannose receptor and PKC: implications for multiple sclerosis. *Acta Neuropathol. Commun.* 3:45. doi: 10.1186/s40478-015-0223-1

Kornberg, M. D., Smith, M. D., Shirazi, H. A., Calabresi, P. A., Snyder, S. H., and Kim, P. M. (2018). Bryostatin-1 alleviates experimental multiple sclerosis. *Proc. Natl. Acad. Sci.* 115, 2186–2191. doi: 10.1073/pnas.1719902115

Kozikowski, A. P., Wang, S., Ma, D., Yao, J., Ahmad, S., Glazer, R. I., et al. (1997). Modeling, chemistry, and biology of the benzolactam analogues of indolactam V (ILV). 2. Identification of the binding site of the benzolactams in the CRD2 activator-binding domain of PKCδ and discovery of an ILV analogue of improved isozyme selectivity. *J. Med. Chem.* 40, 1316–1326. doi: 10.1021/jm960875h

Kutzelnigg, A., and Lassmann, H. (2014). Pathology of multiple sclerosis and related inflammatory demyelinating diseases. *Handb Clin Neurol.* 122, 15–58. doi: 10.1016/B978-0-444-52001-2.00002-9

Laird, G. M., Bullen, C. K., Rosenbloom, D. I. S., Martin, A. R., Hill, A. L., Durand, C. M., et al. (2015). Ex vivo analysis identifies effective HIV-1 latency-reversing drug combinations. *J. Clin. Invest.* 125, 1901–1912. doi: 10.1172/JCI80142

Lim, P. S., Sutton, C. R., and Rao, S. (2015). Protein kinase C in the immune system: from signalling to chromatin regulation. *Immunology* 146, 508–522. doi: 10.1111/imm.12510

Loy, B. A., Lesser, A. B., Staveness, D., Billingsley, K. L., Cegelski, L., and Wender, P. A. (2015). Toward a biorelevant structure of protein kinase C bound modulators: design, synthesis, and evaluation of labeled bryostatin analogues for analysis with rotational echo double resonance NMR spectroscopy. *J. Am. Chem. Soc.* 137, 3678–3685. doi: 10.1021/jacs.5b00886

Mahad, D. H., Trapp, B. D., and Lassmann, H. (2015). Pathological mechanisms in progressive multiple sclerosis. *Lancet Neurol.* 14, 183–193. doi: 10.1016/S1474-4422(14)70256-X

Newton, A. C. (2018). Protein kinase C: perfectly balanced. *Crit. Rev. Biochem. Mol. Biol.* 53, 208–230. doi: 10.1080/10409238.2018.1442408

Noh, K. T., Son, K. H., Jung, I. D., Kang, H. K., Hwang, S. A., Lee, W. S., et al. (2012). Protein kinase C δ (PKCδ)-extracellular signal-regulated kinase 1/2 (ERK1/2) signaling Cascade regulates glycogen synthase Kinase-3 (GSK-3) inhibition-mediated Interleukin-10 (IL-10) expression in lipopolysaccharide (LPS)-induced endotoxemia. *J. Biol. Chem.* 287, 14226–14233. doi: 10.1074/jbc.M111.308841

Platten, M., Eitel, K., Wischhusen, J., Dichgans, J., and Weller, M. (2003). Involvement of protein kinase and extracellular signal-regulated kinase-2 in the suppression of microglial inducible nitric oxide synthase expression by N-[3,4-dimethoxycinnamoyl]-anthranilic acid (tranilast). *Biochem. Pharmacol.* 66, 1263–1270. doi: 10.1016/S0006-2952(03)00449-0

Reich, D. S., Lucchinetti, C. F., and Calabresi, P. A. (2018). Multiple Sclerosis. *N. Engl. J. Med.* 378, 169–180. doi: 10.1056/NEJMra1401483

Rolfe, A. J., Bosco, D. B., Broussard, E. N., and Ren, Y. (2017). In vitro phagocytosis of myelin debris by bone marrow-derived macrophages. *J. Visual. Exp.* 130:e56322. doi: 10.3791/56322

Sloane, J. L., Benner, N. L., Keenan, K. N., Zang, X., Soliman, M. S. A., Wu, X., et al. (2020). Prodrugs of PKC modulators show enhanced HIV latency reversal and an expanded therapeutic window. *Proc. Natl. Acad. Sci. U. S. A.* 117, 10688–10698. doi: 10.1073/pnas.1919408117

Smith, M. E., van der Maesen, K., Somera, F. P., and Sobel, R. A. (1998). Effects of phorbol myristate acetate (PMA) on functions of macrophages and microglia in vitro. *Neurochem. Res.* 23, 427–434. doi: 10.1023/a:1022478005243

Sun, M.-K., and Alkon, D. L. (2006). Bryostatin-1: pharmacology and therapeutic potential as a CNS drug. *CNS Drug Rev.* 12, 1–8. doi: 10.1111/j.1527-3458.2006.00001.x

Tanaka, J. (2000). Nasu-Hakola disease: a review of its leukoencephalopathic and membranolipodystrophic features. *Neuropathology* 20, 25–29. doi: 10.1046/j.1440-1789.2000.00297.x

Ulland, T. K., and Colonna, M. (2018). TREM2 — a key player in microglial biology and Alzheimer disease. *Nat. Rev. Neurol.* 14, 667–675. doi: 10.1038/s41582-018-0072-1

Voet, S., Prinz, M., and van Loo, G. (2018). Microglia in central nervous system inflammation and multiple sclerosis pathology. *Trends Mol. Med.* 25, 112–123. doi: 10.1016/j.molmed.2018.11.005

Wang, S., Sudan, R., Peng, V., Zhou, Y., du, S., Yuede, C. M., et al. (2022). TREM2 drives microglia response to amyloid-β via SYK-dependent and -independent pathways. *Cell* 185, 4153–4169.e19. doi: 10.1016/J.CELL.2022.09.033

Wender, P. A., Cribbs, C. M., Koehler, K. F., Sharkey, N. A., Herald, C. L., Kamano, Y., et al. (1988). Modeling of the bryostatins to the phorbol ester pharmacophore on protein kinase C. *Proc. Natl. Acad. Sci. U. S. A.* 85, 7197–7201. doi: 10.1073/pnas.85.19.7197

Wender, P. A., Koehler, K. F., Sharkey, N. A., Dell'Aquila, M. L., and Blumberg, P. M. (1986). Analysis of the phorbol ester pharmacophore on protein kinase C as a guide to the rational design of new classes of analogs. *Proc. Natl. Acad. Sci. U. S. A.* 83, 4214–4218. doi: 10.1073/pnas.83.12.4214

Xie, M., Liu, Y. U., Zhao, S., Zhang, L., Bosco, D. B., Pang, Y. P., et al. (2022). TREM2 interacts with TDP-43 and mediates microglial neuroprotection against TDP-43-related neurodegeneration. *Nat. Neurosci.* 25, 26–38. doi: 10.1038/s41593-021-00975-6

Yi, P., Schrott, L., Castor, T. P., and Alexander, J. S. (2012). Bryostatin-1 vs. TPPB: dose-dependent APP processing and PKC-α, −δ, and -ε isoform activation in SH-SY5Y neuronal cells. *J. Mol. Neurosci.* 48, 234–244. doi: 10.1007/s12031-012-9816-3

Zheleznyak, A., and Brown, E. J. (1992). Immunoglobulin-mediated phagocytosis by human monocytes requires protein kinase C activation. Evidence for protein kinase C translocation to phagosomes. *J. Biol. Chem.* 267, 12042–12048. doi: 10.1016/s0021-9258(19)49803-7